RSC Advances

ROYAL SOCIETY OF CHEMISTRY

www.rsc.org/advances

Table of Contents

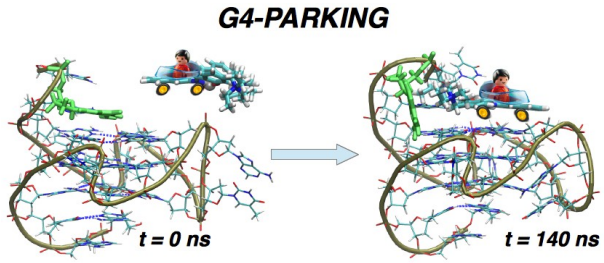

Molecular dynamics simulations and quantum mechanics/molecular mechanics calculations provided a mechanism for G-quadruplex binding of three transition metal complexes

ARTICLE TYPE www.rsc.org/xxxxxx | XXXXXXXX

Selective G-Quadruplex Stabilizers: Schiff-base Metal Complexes with Anticancer Activity

Alessio Terenzi,[a] Riccardo Bonsignore,[a] Angelo Spinello,[a] Carla Gentile,[a] Annamaria Martorana,[a] Cosimo Ducani,[b] Björn Högberg,[b] Anna Maria Almerico,[a] Antonino Lauria[a] and Giampaolo Barone*[a,c]

Received (in XXX, XXX) Xth XXXXXXXXX 200X, Accepted Xth XXXXXXXXX 200X
First published on the web Xth XXXXXXXXX 200X
DOI: 10.1039/b00000000x

The affinity of three square-planar nickel(II) (**1**), copper(II) (**2**) and zinc(II) (**3**) Schiff-base complexes for wild-type human telomeric (*h-Telo*) and protooncogene *c-myc* G-quadruplex (G4) DNA was investigated by UV-visible absorption spectroscopy and circular dichroism. DNA-binding constants (K_b) were determined by spectrophotometric titrations for both G4-DNA and B-DNA. The results obtained point out that the three metal complexes selectively bind G4-DNA with higher affinity, up to two orders of magnitude, with respect to B-DNA. The nickel(II) complex **1** was found to be the most effective G4-DNA stabilizer and the K_b values decrease in the order **1** > **2** ≈ **3**. Innovative computational investigations, consisting of molecular dynamics (MD) simulations followed by density functional theory/molecular mechanics (DFT/MM) calculations, provide an atomistic support for the interpretation of the binding mechanism to G4-DNA by end stacking and also of the experimental affinity order. Interestingly, **1** is able to induce G4-DNA formation of *h-Telo* sequences, also in the absence of K^+ cations. This last result is nicely confirmed and highlighted by polymerase chain reaction (PCR) stop assays, which show the ability of the title compounds to induce and stabilize G4 structures inhibiting the amplification of PCR products. Finally, compounds **1**-**3** showed concentration and time-dependent cytotoxicity towards HeLa and MCF-7 human cancer cell lines, inducing significant effects on cell cycle distribution with G2/M arrest in HeLa cells and G0/G1 arrest in MCF-7 cells. Overall, the PCR inhibition and anticancer activity of the three compounds decreases in the same order **1** > **2** ≈ **3**, in excellent correlation with the G4-DNA-binding affinity, implying that G4-DNA is the biotarget for their biological activity.

1. Introduction

Since the discovery by Rosenberg *et al.* that cisplatin is a highly effective anticancer agent,[1] DNA was considered a major target for anticancer drugs, and actually is the target of the most common clinically used platinum-based drugs.[2] Unluckily, platinum anticancer drugs, which covalently bind the polynucleotide, often present serious side-effects. For such reason, in the last 40 years there was a growing research interest in the study of DNA non-covalent recognition by small molecules.[3–6]

Despite many of these compounds have been extensively studied and some of them clinically used,[3,7] their serious side effects and lack of selectivity resulted in a gradual loss of interest. DNA has lost his initial "appeal" as target mainly due to the discover of more specific cellular targets like proteins, enzymes and cell surface receptors, among others.[8–12]

Nevertheless, new findings in DNA non-canonical structural arrangements with possible roles in carcinogenic events gave to DNA-based drugs a new impetus.[13–15] Telomeres, for instance, are able to organize themselves in four-stranded DNA structures, termed guanine-quadruplexes (G4). G4s, in general terms, can be defined as G-rich sequences capable of forming highly polymorphic 4-stranded structures organized in stacked guanine tetrads connected by looping DNA bases and stabilized by a central alkali ion channel.[16] The propensity of a sequence to fold into a particular secondary structure is influenced by a number of factors including the nature of the central ion, the relative direction of the strands, the *syn* or *anti* glycosidic conformation, the length of the sequence connecting the strands (i.e. the loops) and, in general terms, by the folding experimental conditions.[16–18]

G4s in telomeres were found to be involved in maintaining chromosome stability through the inhibition of telomerase, a ribonucleoprotein complex with reverse transcriptase activity,[19] which turns on to elongate the telomeric overhangs, with a corresponding extension of the cell life. Indeed, telomerase is over-expressed in ca. 80−85% of cancer cells and is responsible of their immortalization. Hence, the inhibition of telomerase, through the folding of its substrate in G4 conformation, is nowadays considered a smart and selective anticancer strategy.[20]

As human genome presents approximately 350,000 guanine-rich sequences,[21] it is not strange the finding that G4-DNA structures are over-represented not only in telomeres but also in gene promoter regions, making them even more attractive as therapeutic targets in oncology.[8] For example, the proto-oncogene *c-myc* presents a putative G4-DNA in the nuclease hypersensitive element (NHE).[22,23] The aberrant overexpression of *c-myc* is associated with a variety of malignant cancers.[22] Folding patterns of several G4s motifs in

promoter regions, described as possible molecular switch in transcriptional regulation,[8] have been proposed, including *c-myc*, *c-kit*, *KRAS*, *PDGF-A*, *hTERT* and HIF.[8,21,24] Futhermore, recent works emphasize that G4 structures were found also in RNA G-rich sequences, and that they seem to play a key role in post-transcriptional control of gene expression.[25]

Many research groups have worked to identify or design small-molecule ligands, which specifically bind to the G4-DNA inhibiting cell proliferation.[16–18,26] To date, molecules able to stabilize a G4 structure present specific features, like a π-delocalised system in order to π-stack with the terminal G-quartets and positively charged substituent able to interact with the grooves. It has been recently reported that planar aromatic organic molecules complexed with transition metal ions are attractive systems for quadruplex binding.[20,27,28] The presence of a metal ion, due to an electronwithdrawing effect, reduces the electron density on the coordinated aromatic ligands and induces stronger π interactions with the G-quartets.[20] Furthermore, the metal ion increases the electrostatic G4 stabilization by positioning at the center of a G-tetrad and ideally continuing the central ion channel normally created by alkali metal cations.[27]

The principal effort in G4-DNA binders design concerns target selectivity. The ideal ligand should bind a G4-DNA structure with high affinity and recognize specifically the G4-DNA in preference to the duplex B-DNA.[29]

Cationic Salphen-like metal complexes, already known to be B-DNA binders,[30–32] represent a powerful class of G4-DNA stabilizers.[20] For istance, Vilar *et al.* reported the synthesis of a series of square planar transition metal complexes with salphen-like N,N'-bridged tetradentate ligands with a surprisingly ability to stabilize human telomeric DNA with considerable affinity and selectivity.[33,34]

With the aim to extend the library of Schiff-base G4-binding metal complexes and to increase their selectivity over B-DNA, three square-planar cationic complexes, ML^{2+} (M = Ni, Cu, and Zn), recently synthesized and characterized by an extended nearly planar area (Fig. 1),[35] have been tested as G4 stabilizers and their binding affinity compared to that toward B-DNA. Circular dichroism (CD) and UV-visible (UV-vis) absorption spectroscopy allowed us to monitor the metal complex-G4 interaction and to discriminate the quadruplex fold from other architectures. Computational chemistry methods have been used to provide atomistic models of the supramolecular metal complex-G4 binding complexes.

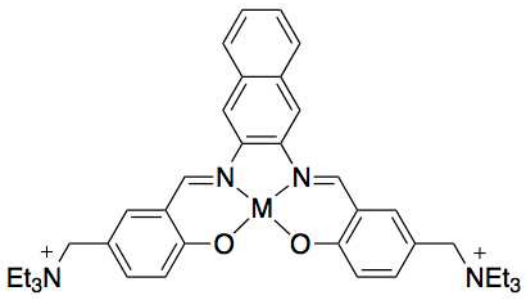

Fig 1. Structure of the ML^{2+} complex (**1**: M=Ni, **2**: M=Cu; **3**: M=Zn; H_2L^{2+} = 5-triethyl ammonium methyl salicylidene *ortho*-naphthalenediimine).

We have taken our studies further to demonstrate the effect of the selected compounds on the DNA processing through *in vitro* polymerase chain reaction (PCR) assays. Moreover, we have evaluated the related antiproliferative activity towards HeLa and MCF-7 cancer cell lines.

2. Results and discussion

2.1. Absorption spectroscopy

To investigate the DNA recognition properties of compounds **1-3** and, in particular, their selectivity towards G4-DNA, UV-vis titrations with 5'-$(AGGGTT)_3$AGGG-3' (*h-Telo* G4), 5'-GGGAGGGTGGGGAGGGTGGG-3' (*c-myc* G4) and ct-DNA were performed (Figs. 2 and S1 of the Supplementary Information).

Compounds **1-3** present a metal center in a +2 oxidation state but differing for the number of *d* electrons and share an intense absorption band at about 250 nm (black solid lines in Fig. 2a,b,c). Moreover, characteristic absorption bands are noticeable in **1** (346 and 467 nm), **2** (316 and 406 nm) and **3** (304 and 384 nm).

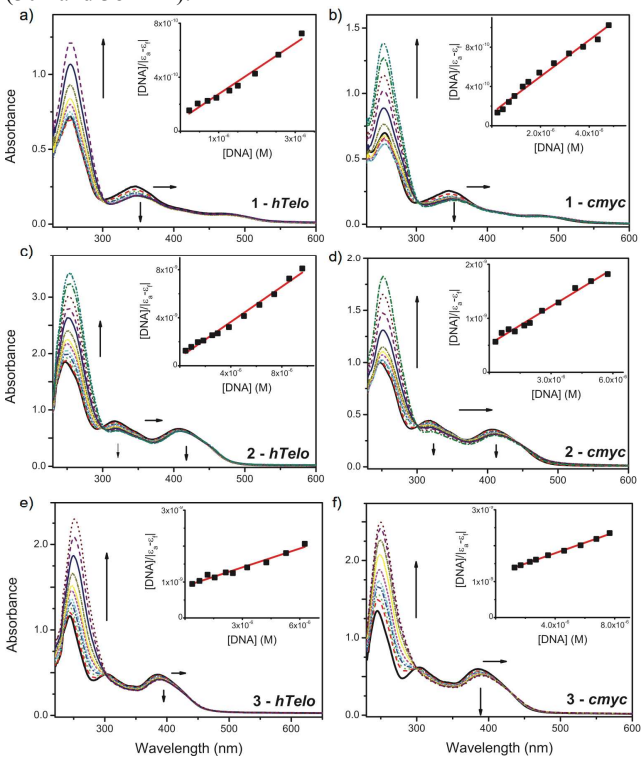

Fig 2. Absorption spectra of **1** (a, b), **2** (c, d) and **3** (e, f), in presence of increasing amounts of *h-Telo* G4-DNA (left column) and *c-myc* G4-DNA (right column) in Tris-HCl buffer 50 mM and KCl 100 mM. (a) [**1**] = 13.4 μM, (b) [**1**] = 13.7 μM, (c) [**2**] = 35.1 μM, (d) [**2**] = 19.4 μM, (e) [**3**] = 21.8 μM, (f) [**3**] = 27.3 μM. Ratios R = [DNA]/[ML^{2+}] are in the range 0.00-0.30 for all the titrations. The arrows indicate the change upon G4-DNA addition.

Such spectra are significantly modified by the addition of increasing amounts of the selected *h-Telo* and *c-myc* G4 oligonucleotides (Fig. 2). The addition of increasing amounts of G4-DNA produces a considerable hypochromic and bathochromic effect of the metal complex intraligand π-π* band. In detail, a hypochromic effect of about 24% for

compounds **1-2**, and of 14% for **3** is observed, with a red shift of about 4 nm for the three metal complexes. The results, almost identical for *h-Telo* and *c-myc*, are in agreement with an end-stacking binding mode.[36] Structural details of the metal complex-G4 interaction, nicely explaining the observed spectroscopic properties, were obtained by the computational studies discussed below.

The B-DNA binding abilities by intercalation of the synthesized metal complexes are already known from our studies recently published.[35] However, to be quantitatively compared, the titrations with ct-DNA and G4-DNA have been performed by using the same experimental conditions. In particular, it is known that the ionic strength of the medium strongly affects the interaction of the negatively charged double helical polymer and the positively charged molecules.[37] The effect of ionic strength on the binding constant can be rationalized by the Record equation,[38] in which the decrease of the binding constant, $\Delta(\log K)$ versus the incremental ionic strength, $\Delta(-\log I)$, must be linear.

In details, the absorption band of **1** at 346 nm (black line in Fig. S1a) is red shifted by about 5 nm and shows hypochromism of about 26%. The absorption band of **2** at 316 nm (black line in Fig. S1b) is red shifted by about 5 nm and shows hypochromism of about 22%. Finally, the absorption band of **3** at 304 nm (black line in Fig. S1c) is red-shifted by about 3 nm and shows hypochromism of about 11.9%. These results, mainly caused by stacking interaction between the extended aromatic rings of the Schiff-base metal complexes and the base pairs of DNA,[37,39,40] collectively confirm that **1-3** act as DNA intercalators also at high ionic strength conditions.

To determine the intrinsic binding constant (K_b) of the ML^{2+}/DNA systems, the quantity $[DNA]/|\varepsilon_a-\varepsilon_f|$ at 346 nm for **1**, at 407 nm for **2** and at 304 nm for **3** nm has been plotted, as a function of the molar concentration of DNA (insets in Figs. 2 and S1). The binding constants were obtained by fitting the data to a reciprocal plot of $[DNA]/|\varepsilon_a-\varepsilon_f|$ versus [DNA] using the following equation:[20]

$$[DNA]/|\varepsilon_a-\varepsilon_f| = [DNA]/|\varepsilon_b-\varepsilon_f| + 1/(|\varepsilon_b-\varepsilon_f| \times K_b) \quad \text{Eq. 1}$$

where the concentration of DNA is expressed in terms of monomer units. In details, $\varepsilon_a = A_{observed}/[ML^2]$, ε_b is the extinction coefficient of the DNA bound complex, and ε_f is the extinction coefficient of the free complex determined by a calibration curve of the isolated metal complexes in aqueous solution, following the Beer-Lambert law. The K_b values obtained by the linear fits of the experimental data using Eq. (1) are reported in Table 1.

Table 1. DNA-binding constants, K_b (M^{-1}), of the three metal complexes **1-3** with G4-DNA (*h-Telo* and *c-myc*) and B-DNA (ct-DNA).

	ct-DNA	*h-Telo*	*c-myc*
1	$(4.430.37)\times10^4$	$(2.160.57)\times10^6$	$(1.540.20)\times10^6$
2	$(1.680.13)\times10^4$	$(2.040.12)\times10^5$	$(4.460.42)\times10^5$
3	$(1.330.14)\times10^4$	$(1.980.21)\times10^5$	$(1.160.28)\times10^5$

These results confirm that each metal complex interacts with both B- and G4- DNA secondary structures and that the binding of Ni^{II} complex is tighter than Cu^{II} which is tighter than Zn^{II}, following the order **1** > **2** ≈ **3**. Most importantly, the three compounds show binding selectivity for G4 structures. In fact, while the binding constant of compounds **2** and **3** for both *h-Telo* and *c-myc* G4-DNA is about 10 times higher than that for ct-DNA, this value increases to about 100 times higher for the nickel(II) compound **1**. In this respect, it has been recently reported that, to achieve sequence-specific DNA targeting, the ideal binding affinity between specific and nonspecific sites should be approximately 1000 times.[41] However, such selectivity was up to date not yet reached. For example, highly active telomerase inhibitors bind to human quadruplex DNA only 30-40 times more strongly than to duplex DNA.[42] By a comparison with the binding data so far reported, this means that the binding selectivity reached by the nickel(II) compound is greater than that obtained for most selective G4-binders known up to date.

2.2. Circular dichroism

CD is an essential method for the structural characterization of G4-DNA in solution. This technique is highly sensitive to little variations of the chiral conformation of an optically active biomolecule.[43–45] In G4-DNA the chromophores absorbing in the UV-Vis region are represented by guanines, with two well-isolated absorption bands which are connected to two well characterized short and long axis polarised π–π* transitions at ca. 279 nm and 248 nm. The fact that the stacked G-tetrads are rotated one with respect to the others causes chiral exciton coupling between transition dipole moments located in near-neighbour guanines. This chiral DNA structure is thus active for CD studies and drug–DNA interactions can be monitored.[46]

Although there are many quadruplex structures available, only three basic types of CD spectra exist, which have been associated to three groups representative of all possible quadruplex topologies. The first one (group I) contains only parallel G4s, with strands that progress in the same direction and characterized by guanosines of the same glycosidic bond angle (*syn-syn* or *anti-anti*). Antiparallel quadruplexes with consecutively stacked guanosines of distinct glycosidic bond angle (i.e. *syn-anti-syn*) belong to group III. The others antiparallel hybrid structures belong to group II.[44]

In 100 mM KCl solution, telomeric DNA exhibits a mixture of parallel and antiparallel structures and it has been previously shown that some G4-DNA binders can induce preferentially one of the two conformations.[47–49] The typical group II CD spectrum of *h-Telo* consists of a characteristic positive band centered at 290 nm with a shoulder at 270 nm (black solid line in Fig. 3a,c,e).[50]

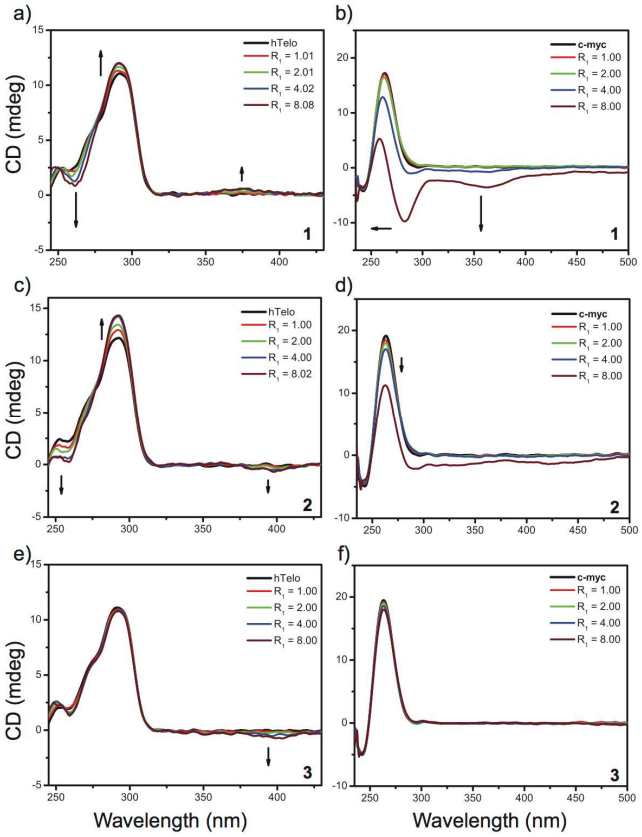

Fig 3. Circular dichroism spectra of *h-Telo* G4-DNA (a,c,e) and *c-myc* G4-DNA (b,d,f) in presence of increasing amounts of **1** (a,b), **2** (c,d), **3**, (e,f) in 50 mM Tris-HCl (pH=7.5) and 100 mM KCl. (a) [*h-Telo*] = 3.0 μM. (b) [*c-myc*]= 2.0 μM, c) [*h-Telo*] = 3 μM, (d) [*c-myc*] = 2.0 μM. (e) [*h-Telo*]= 3.0 μM, f) [*c-myc*] = 2 μM. Ratios $R_1 = [ML^{2+}]/[DNA]$ are reported in the legend.

Upon addition of increasing amounts of **1** to *h-Telo* DNA, a slight intensification of the band at 295 nm occurs together with an attenuation of that at 265 nm (Fig. 3a). Comparing this result with those reported in the literature,[28,47] it is possible to conclude that the nickel complex **1**, in 100 mM KCl buffered solutions, induces conformational changes favoring the anti-parallel conformation of *h-Telo* G4-DNA, with a possible switch from a group II to a group III structure. Almost the same results can be observed for the copper complex **2** (Fig. 3c), while **3** interacts with the quadruplex, as shown by the negative induced CD (ICD) band appearing at around 400 nm, but with no preference for parallel or anti-parallel conformation (Fig. 3e).

An intense positive band at 263 nm and a negative band at approximately 240 nm of the *c-myc* oligomer (black solid line in Fig. 3b,e,f) is a typical fingerprint of a parallel G4 structure belonging to group I.[23,51] The addition of increasing amounts of **1** and **2** results in a decrease of this band indicating again a preference over an antiparallel structure (Fig. 4b,d, respectively). Compound **3** seems to stabilize the parallel structure as it is.

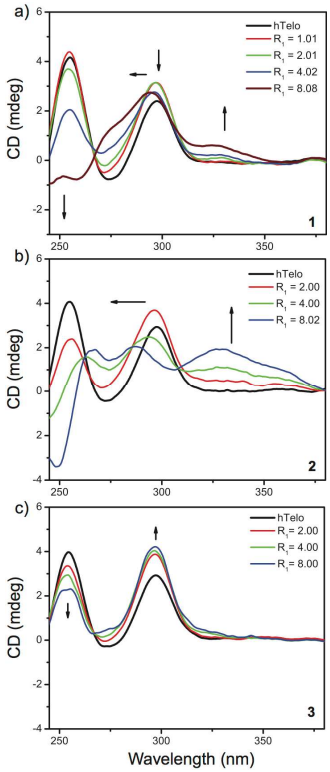

Fig 4. Circular dichroism spectra of unfolded 5'-$(AGGGTT)_3$AGGG-3' *h-Telo* DNA in presence of increasing amounts of **1** (a), **2** (b) and **3** (c) in 50 mM Tris-HCl (pH=7.5) [*h-Telo*] = 3.0 μM. Ratios $R_1 = [ML^{2+}]/[DNA]$ are reported in the legend.

We have also checked the ability of complexes **1-3** to induce the formation of G4-DNA in the absence of potassium cations, by measuring the CD of *h-Telo* DNA in a KCl free buffer. Non-annealed *h-Telo* DNA shows the characteristic positive ellipticity at ca. 250 nm consistent with a singly stranded DNA sequence (see black line in Fig. 4 or red line in Fig. 5). While the addition of the zinc complex **3** only slowly perturbs the CD spectra of linear *h-Telo*, upon addition of increasing amounts of **1** and **2**, significant changes are observed. In detail, the positive band centered at 255 nm, associated with the non-annealed *h-Telo* DNA, decreases and a positive ICD band appears at about 330 nm. Remarkably, the addition of the nickel complex **1** induces also an increase of the positive peaks at 295 nm and of the shoulder at 265 nm, indicative of the formation of antiparallel and of parallel G4-DNA, respectively (see Fig. 4 and 5). This result indicates that complex **1** is able to induce the formation of G4-DNA even in the absence of K^+ cations.

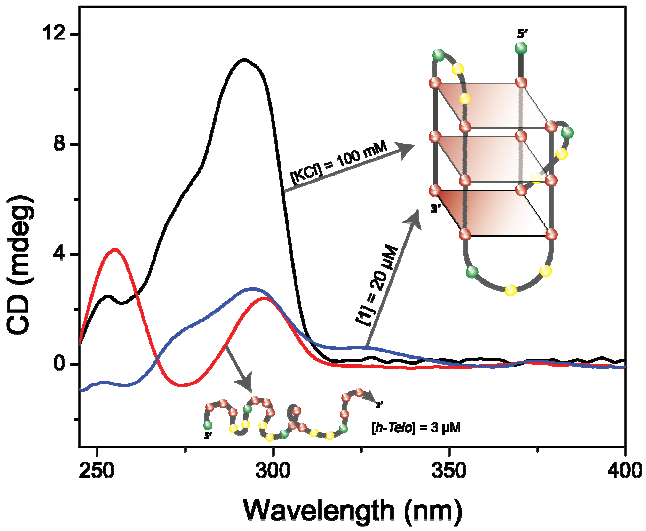

Fig 5. Circular dichroism spectra of unfolded 5'-(AGGGTT)$_3$AGGG-3' *h-Ttelo* 3 μM (red line), G4 folded in presence of K^+ 100 mM (black line) and G4 folded in presence of 20 μM **1**. All spectra were recorded in 50 mM Tris-HCl.

2.3. MD simulations and DFT/MM calculations

MD simulations have been performed on the two complexes between **3** and both *c-myc* and *h-Telo* sequences in G4-DNA conformation. The root mean square deviations (RMSD) along the simulation, for all non-hydrogen atoms and for the guanine bases, are shown in Fig. 6 and S2 of the Supplementary Information, respectively. The results of the MD simulations show that the strong interaction between the zinc(II) complex **3** and both G4-DNA models is driven by the strong electrostatic attraction between the positively charged triethylammoniummethyl groups of the Schiff-base ligand and the negatively charged phosphate groups of the biomolecule. This long-range interaction allows the metal complex to easily approach the biomolecule. Moreover, a strong π-π stacking interaction occurs at the equilibrium, between the naphthalene moiety of the Schiff-base ligand and the terminal G-tetrad. The three snapshots reported in the RMSD plot in Fig. 6 nicely describe the dynamics of the approaching of the zinc(II) complex toward the *c-myc* G4 structure. In particular, it is worth noting that the guanine basis lying above the terminal G-tetrad, colored in green, performs a rotation of about 90° around its glycosidic bond and that the larger rotation is abruptly obtained at about 100 ns, as highlighted by the step in the RMSD of the guanine bases (red line in Fig. 6). This rotation allows a suitable stacking interaction between the naphthalene moiety of the metal complex and the G-tetrad of *c-myc* G4-DNA. The binding mechanism can be appreciated also by looking at the supplementary video file video.mpg **{PLEASE INSERT A HYPERLINK TO METAFILE video.mpg}**, with a hyperlink in the online version of this paper, which shows a movie of the molecular dynamics described in Fig. 6.

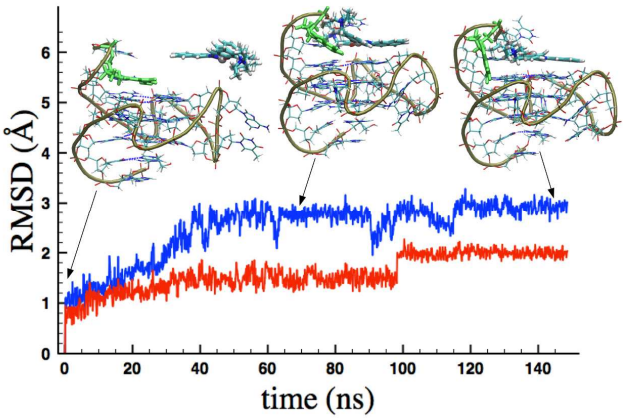

Fig 6. Plot of the RMSD obtained for **3**/*c-myc* up to 150 ns of MD simulations.

Concerning the interaction with the *h-Telo* G4, the RMSD plot in Fig. S2 shows that the equilibrium is quickly reached at about 5 ns and the stacked metal complex remains tightly bound to the biomolecule up to the end of the MD simulation. The equilibrium geometry, after about 50 ns, has been used as starting point for further geometry optimizations, by hybrid two-layer QM/MM calculations, using DFT as QM method and the Amber99 force field as MM method, as recently reported,[52] of the intercalation complexes of the three metal complexes **1**-**3** with *h-Telo* in G4 conformation (Fig. 7). The higher layer of the DFT/MM structures involves the four guanine bases of the G-tetrad and the metal complex. The optimized structures shown in Fig. 7 provide interesting atomistic details of the binding complexes, explaining the strong DNA-binding experimentally detected. In particular, the metal ion of the three Schiff-base complexes is almost in line with the two potassium cations in the central channel formed by the three stacked G-tetrads. Moreover, metal coordination occurs in **2**/*h-Telo* and **3**/*h-Telo*, by one of the four O6 keto oxygen atoms of the guanine bases, as reported in Fig. 7. Such metal coordination and the concomitant distortion of the square planar geometry of the complexes, that decreases in the order Zn > Cu > Ni, together with consideration on solvent and thermodynamic contributions, provide an explanation of the decreasing affinity order, Ni > Cu ≈ Zn, experimentally detected, between the three complexes and G4-DNA.

In fact, standard enthalpy and Gibbs free energy values, calculated at 298.15 K, were used to evaluate, *in vacuo* and in solution, the formation energy of the supramolecular complexes between **1**, **2** and **3** with *h-Telo* G4-DNA (Table 2). The tabulated data allow us to make interesting considerations of the energetic contributions involved in the G4-DNA binding of the title metal complexes, analogous to that recently reported for the binding of the three metal complexes with B-DNA.[35]

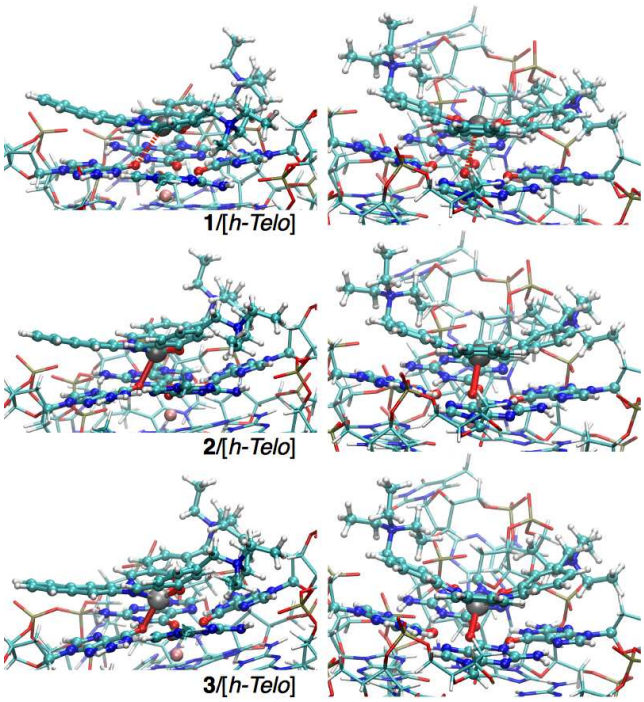

Figure 7. Two different views of the binding site of the supramolecular complexes between the three metal complexes **1**-**3** with *h-Telo* G4, highlighting the interatomic distances of the metal ion with one of the four O6 keto atoms of guanine (in red, 3.12 Å (**1**), 2.46 Å (**2**) and 2.12 Å (**3**)). DFT and MM regions are represented by "ball and stick" and "sticks" styles, respectively.

First, the binding with the biomolecule is always accompanied by a strong exothermic contribution, both *in vacuo* and in solution. However, both entropy and solvation play a destabilizing effect on the DNA-binding energy. The role of the polar solvent can be rationalized taking into account that there is a considerable electrostatic character in the interaction energy, which is screened going from the gas phase to water solution. The solvent destabilization decreases in the order Zn > Cu > Ni, in parallel with the decrease of the calculated APT charges, *in vacuo*, of the three ions in the binding complexes shown in Fig. 7, 1.61, 1.34 and 1.04, for Zn, Cu and Ni, respectively. The formation free energy is always smaller than the formation enthalpy, both *in vacuo* and in solution, indicating that the entropic contribution, in the equation $\Delta G° = \Delta H° - T\Delta S°$, is always negative. However, such entropic destabilization is lower for the complexes of *h-Telo* with the nickel complex **1** and higher for that with the copper and zinc complexes **2** and **3**. The latter result is in our opinion related to the existence of a chemical bond between the exocyclic keto oxygen O6 and both the copper and zinc ions in **2**/*h-Telo* and **3**/*h-Telo*, while this coordination bond does not form with the nickel ion in **1**/*h-Telo* (see Fig 7). Finally, the calculated formation free energy values in solution, -34.6, -14.4 and -20.9 kJ/mol, are in good agreement with the experimental values, -36.2, -30.3 and -30.2 kJ/mol, obtained by the equation $\Delta G°=-RT \ln (K_b)$ and using the K_b values reported in Table 1 for the interaction of **1**, **2** and **3** with *h-Telo* G4-DNA.

Table 2. Formation energy,[a] in kJ/mol, in terms of standard enthalpy (ΔH°) and Gibbs free energy (ΔG°), calculated at 298.15 K for the complexes of **1**, **2** and **3** with *h-Telo* G4-DNA.

Model system	ΔH° (vacuo)	ΔG° (vacuo)	ΔH° (water)	ΔG° (water)
1/*h-Telo*	-233.9	-122.6	-145.9	-34.6
2/*h-Telo*	-242.5	-107.6	-149.2	-14.4
3/*h-Telo*	-290.9	-154.9	-156.8	-20.9

[a] The formation energy was evaluated by the following equation, where E can be either H or G: $E° = E°(ML^{2+}/G4\text{-}DNA) - E°(G4\text{-}DNA) - E°(ML^{2+})$.

2.3. Biological Activity

Spectroscopic analysis of the interaction of ML^{2+} complexes with DNA showed that the complexes behave as typical intercalators and bind effectively to G4. Thus, to elucidate the consequences of the cell exposure to those DNA-binders, the three ML^{2+} complexes were tested for the antiproliferative activity and in cell cycle perturbation experiments on HeLa and MCF-7 cancer cell lines.[53,54]

2.3.1. Antiproliferative Activity

Antiproliferative activity of compounds **1**-**3** was tested using MTT based cell viability assay. All compounds showed concentration-dependent and time-dependent growth inhibition activity toward both cancer cell lines, but the effect was achieved with diverse efficacy. In general, **2** and **3** showed modest antiproliferative effects whereas **1** was the most active.

The GI50 values of **1**-**3** tested at 24 h and 48 h are shown in Table 3.

Table 3. Time-dependent anticancer activity - GI50 ± SE (μM). Cytotoxicity expressed as GI50 values of ZnL^{2+}, CuL^{2+} and NiL^{2+} in HeLa and MCF-7 cell lines.

		HeLa	MCF-7
1	**24h**	16.54 ± 1.72	9.80 ± 0.81
	48h	0.31 ± 0.07	1.42 ± 0.08
2	**24h**	22.32 ± 1.36	29.26 ± 2.36
	48h	10.15 ± 0.94	13.58 ± 1.22
3	**24h**	> 50	> 50
	48h	13.04 ± 1.42	21.94 ± 2.04

3 showed low cytotoxic effects against both tested cell lines and displayed at 24 h GI50 values > 50 μM and at least 80% cell viability. At 48 h no significant difference in GI50 values was observed between **2** and **3** on HeLa cells (10.15 ± 0.94 and 13.04 ± 1.42 μM respectively), whereas **2** was more active on MCF-7 cells (13.58 ± 1.22 and 21.94 ± 2.04 μM respectively). **1** showed very strong cytotoxic effect with GI50 at 24 h in the low micromolar range and at 48 h in sub-micromolar range. Moreover at 48 hrs the MCF-7 cell line displayed higher resistance than the HeLa cells to both **1** and **3**. Higher cytotoxicity of compound **1** may indicate that its mode of action might differ from those of the other active compounds and this result is in agreement with DNA interaction studies in which **1** resulted the best G4-DNA

stabilizer.

2.3.2. Cell cycle perturbation experiments

Anticancer effects can be achieved by cell death and/or cell cycle arrest. The treatment with compounds **1-3** in the range 25 – 0.1 μM did not yield necrosis in MCF7 and HeLa cells, as demonstrated by negative response to LDH activity assay (data not shown). A flow cytometric analysis was carried out to clarify the influence of the title compounds on cell-cycle distribution, and in addition to the cell viability studies. Cell cycle analysis was performed after 48 h of incubation and the working concentration of **1-3** were fixed at 1x and 2x their GI50 values. All tested compounds achieved significant effects ($p < 0.05$) on cell cycle distribution (Fig. 8).

Strong suppression of the G1/G0 phase with cell cycle arrest in the G2/M phase was observed in HeLa cells. In contrast, in MCF-7 compounds induced early arrest with accumulation of cells in the G0/G1 or/and S phases with a G2/M phase reduction. Moreover, a significant cell population increase in the sub-G1 phase was observed, which is indicative of apoptotic cells. The distinct cell cycle arrest phase observed in cells treated with **1-3** might be due to the different consequences of their DNA-binding properties in different cancer cells.[53]

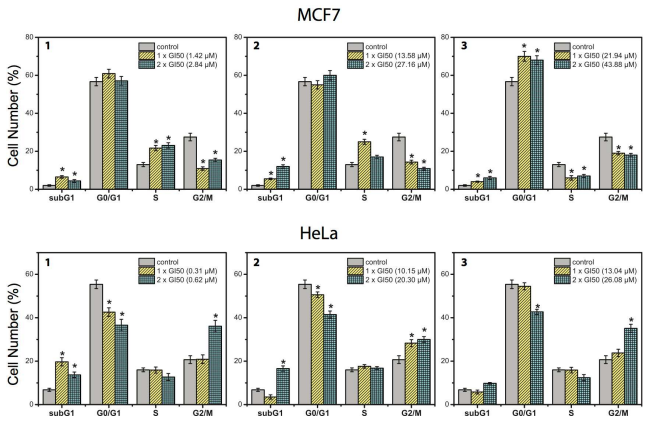

Fig 8. Effects of **1**, **2** and **3**, at 2x and 1x, of their GI50 values on the cell cycle distribution of MCF-7 and HeLa cells at 48 h of treatment. The histograms represent the percentages of cells in the respective cell cycle phase (G1, S, and G2/M), along with the percentage of cells in the subG1 (dead cells) obtained by flow cytometry. Results are expressed as the mean of two independent experiments, performed in duplicate ±SE. Statistical analyses were performed using the Student's t test to determine the differences between the datasets. *$p < 0.05$, denotes significant differences from untreated control cells.

2.4. Stabilizing the G4 structures by polymerase chain reaction (PCR) stop assay

A PCR stop assay was performed to further establish whether the synthesized compounds could induce G4 structures. A test oligonucleotide Pu22myc, corresponding to the NHE III_1 sequence able to form biologically relevant chair G4s but not basket one,[55] was chosen. An induction of its G4 secondary structure mediated by **1-3** would prevent its annealing to a complementary strand overlapping the last G repeat, impeding consequently the elongation of the 3' ends of the oligonucleotides and therefore inhibiting the final double stranded DNA PCR product. The test oligonucleotide and its partially complementary strand were incubated with increasing concentrations of Ni^{II}, Cu^{II} and Zn^{II} complexes for 35 PCR cycles. The final products were visualized on native polyacrylamide gels and they show how all the complexes, though with different efficiency, inhibit the amplification reactions in a dose dependent manner (Fig. 9). In particular the most effective compound is **1**, which is able to achieve an inhibition close to 50% already at 0.2 μM. Also remarkably is the inhibition of **2**, which at only **1** μM induces an inhibition of almost 70%. Finally the last tested compound, **3**, has a lower effect of G4 structure induction, in fact a significant inhibition can be appreciated only at higher concentration (10 and 30 μM). It is important to remark that the PCR inhibition in this assay roughly follows the same trend of the binding constant found by UV-vis experiments performed on the same test oligonucleotides: **1** > **2** > **3**. These results remark the ability of these metal complexes to induce and stabilize G4 structures inhibiting the amplification of PCR products. In addition this assay, differently from previous similar studies,[56] was performed in absence of KCl showing how the tested compounds can induce the G4 structure even without potassium ions in solution.

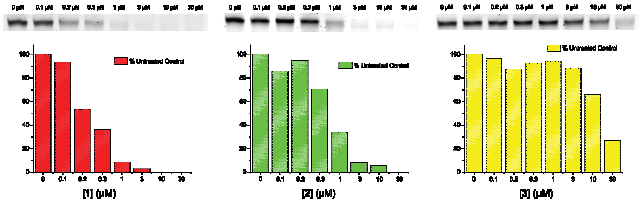

Fig 9. PCR inhibition of Pu22myc with compounds **1**, **2** and **3**.

To further demonstrate that the inhibition induced by the title compounds was mainly due to G4 stabilization of the Pu22myc oligonucleotide, the same assay was performed by replacing the test oligonucleotide Pu22myc with a modified test oligonucleotide, Pu22mu which contains two mutations in one of the guanine repeats. In that case, much higher concentrations were required for inducing an inhibition of the DNA PCR products (see Supplementary Information, Fig. S3). In detail by using Pu22mu, a 30 μM concentration of **1** is necessary for a complete inhibition while in the previous assay performed with Pu22myc, at 1 μM the DNA PCR product is already barely detectable (Fig. 9). Compound **2** similarly induces significant non-specific PCR inhibition only at higher concentrations while **3** does not interfere with the amplification even at highest concentrations.

4. Experimental Section

4.1. General

Solvents and reagents (reagent grade) were all commercial and used without further purification. UV-vis absorption spectra were collected on a Varian Cary 1E double beam

spectrophotometer. Circular dichroism spectra were recorded on a Jasco J-715 spectropolarimeter, using 1 cm path-length quartz cells.

4.2. Synthesis

Compounds **1-3** were synthesized and characterized as recently reported.[35] Briefly, 5-(triethylammoniummethyl) salicylaldehyde chloride in EtOH/H_2O basic solution was added dropwise to an ethanolic solution of 2,3-diaminonaphthalene and the selected metal perchlorate, in a 2:1:1 molar ratio. The solid obtained was collected, washed with cold ethanol and diethyl ether and, finally, recrystallized from ethanol/methanol solutions.

4.3. UV-vis absorption

Lyophilized calf thymus DNA (Fluka, BioChemika) was resuspended in 1.0 mM tris-hydroxymethyl-aminomethane (Tris-HCl) pH=7.5 and dialyzed as described in the literature.[57] DNA concentration, expressed in monomers units ([$DNA_{phosphate}$]), was determined by UV spectrophotometry using 7000 M^{-1} cm^{-1} as molar absorption coefficient at 258 nm.[58] All experiments were carried in 100 mM KCl, 50 mM Tris-HCl aqueous buffer at pH=7.5.

The 22-mer sequence oligonucleotide *h-Telo*: 5'-AGGGTTAGGGTTAGGGTTAGGG-3', and the 20-mer sequence oligonucleotide *c-myc*: 5'-GGGAGGGTGGGGAGGGTGGG-3', were purchased from BioGenerica BioTechnology (Italy). The oligonucleotides were dissolved in MilliQ water to yield a 100 µM stock solution. These were then diluted using 50 mM Tris-HCl/100 mM KCl buffer (pH 7.4) to the desired concentration. The oligonucleotide were folded by heating the solutions up to 90 °C for 5 min and then by slowly cooling at room temperature. The complexes were previously dissolved in dimethyl sulfoxide (DMSO) to give 1 mM stock solutions. These were further diluted using 50 mM Tris-HCl/100 mM KCl to the appropriate concentrations with a final DMSO percentage less than 3%. Concentration of the two oligonucleotides solutions was further checked measuring their absorbance and using the appropriate extinction coefficients, *h-Telo,* ε = 259 mM^{-1} cm^{-1}, *c-myc,* ε = 238 mM^{-1} cm^{-1} as reported in the products labels by BioGenerica BioTechnology.

UV-vis absorption spectra were recorded at 25 °C. The titrations were carried out adding increasing amounts of DNA (ct-DNA or oligonucleotides) stock solution to a metal-complex solution with constant concentration. To ensure that during the titration the concentration of the selected metal complex remained unaltered, for each addition of the DNA solution, the same volume of a double-concentrated metal complex solution was added.

4.4. Circular dichroism

CD spectra were recorded at 25 °C with the following parameters: range 600-200 nm, stop r: 0.2 nm, speed: 200 nm/min, accumulation: 4, response: 0.5 s, bandwidth: 1 nm. The titrations were carried out adding increasing amounts of a metal-complex stock solution to a DNA solution with constant concentration. To ensure that during the titration the concentration of the DNA remained unaltered, for each addition of the complex solution, the same volume of a double-concentrated DNA solution was added.

4.5. Biological Activity

Chemicals and reagents. Propidium iodide, ribonuclease A (RNAse A), 2,5-diphenyl-3-(4,5-dimethyl-2-thiazolyl) tetrazolium bromide (MTT), and DMSO were obtained from Sigma Aldrich (St. Louis, MO, USA). DMEM, RPMI, fetal bovine serum (FBS), phosphate buffered saline (PBS), L-glutamine solution (200 mM), trypsin-EDTA solution (170000 U/l trypsin and 0.2 g/l EDTA) and penicillin-streptomycin solution (10000 U/ml penicillin and 10 mg/ml streptomycin) were purchased from Lonza (Verviers, Belgium).

Cell culture. The cancer cell lines HeLa (human epithelial cervical cancer) and MCF-7 (human epithelial breast cancer), were obtained from American Type Culture Collection (ATCC) (Rockville, MD, USA). The cells were cultured as monolayers and maintained in a humidified atmosphere with 5% CO_2 at 37 °C. MCF-7 cells were grown in DMEM while HeLa cells in RPMI. Both media were supplemented with 5% FBS, 2 mM L-glutamine, 50 IU/ml penicillin, and 50 µg/ml streptomycin. The cells were routinely cultured in 75 cm^2 culture flasks and collected using trypsin-EDTA. Exponentially growing cells were used for experiments.

Antiproliferative Assay. The synthesized complexes **1-3** were submitted to the MTT assay to assess the growth inhibition activity against cancer cell lines. The MTT assay is a measurement of cell metabolic activity, quite effective in estimating cell proliferation, that is based on the protocol first described by Mossmann.[54] The assay was performed as previously described.[53]

The cells were seeded into a series of standard 96-well plates in 100 µl/well of complete culture medium at a plating density depending on the doubling times of individual cell line. MCF-7 cells were seeded at 1.5×10^4 cells/cm^2, while HeLa cells were seeded at 1.0×10^4 cells/cm^2. Cells were incubated for 24 h under 5% CO_2 at 37 °C and the medium was then replaced with 100 µl of fresh medium containing the treatments. The metal-complex stock solutions (20 mM) were prepared by dissolving **1-3** in DMSO. Working solutions were freshly prepared on the day of testing by dilutions of the stock solutions in the complete culture medium. Compounds **1-3** were tested in the 50.0 – 0.1 µM concentration range. 24 h after seeding aliquots of 100 µl of these different metal complex solutions at the appropriate concentrations were added to the appropriate wells and the cells were incubated for 24 h or 48 h, without renewal of the medium. In each experiment, DMSO concentration never exceeded 0.25% and culture medium with 0.25% DMSO was used as control. After the incubation time, cells were washed and 50 µL FBS-free medium containing 0.5 mg/mL of MTT was added. The medium was discarded after a 4-h incubation at 37 °C and formazan blue formed in the cells was dissolved in DMSO. The absorbance (OD, optical density) at 570 nm of MTT-formazan was measured in a microplate reader. As the absorbance is directly proportional to the number of living,

metabolically active cells, the percentage of growth (PG) to respect untreated cell control for each drug concentrations was calculated according to one of the following two expressions:
if $(OD_{test} - OD_{tzero}) \geq 0$, then $PG = 100 \times (OD_{test} - OD_{tzero})/(OD_{ctr} - OD_{tzero})$;
if $(OD_{test} - OD_{tzero}) < 0$, then $PG = 100 \times (OD_{test} - OD_{tzero})/OD_{tzero}$,
where OD_{tzero} is the average of optical density measurements before exposure of cells to the test compound, OD_{test} is the average of optical density measurements after the desired period of time, and OD_{ctr} is the average of optical density measurements after the desired period of time with no exposure of cells to the test compound.
The concentration necessary for 50% of growth inhibition (GI50) for each metal-complex was calculated from concentration−response curves using linear regression analysis by fitting the test concentrations that give PG values above and below the reference value (i.e. 50%). If, however, for a given cell line all of the tested concentrations produced PGs exceeding the respective reference level of effect (PG value of 50), then the highest tested concentration was assigned as the default value, preceded by a ">" sign. Each result was the mean value of three separate experiments performed in quadruplicate.
Cell-cycle analysis. Effects of **1-3** exposure on cell-cycle were assessed by DNA staining with propidium iodide (PI) and flow cytometry analysis. MCF7 and HeLa cells were seeded on 6 well plates at a density of 2.5 10^4 cells/cm^2, and treated 24 hours after seeding with or without test compounds for 48 h. Following the treatments, cells were collected, washed in PBS, fixed in ice-cold 70% ethanol and kept at -20 °C. Fixed cells were centrifuged, resuspended in PBS and incubated with staining solution (20 µg/ml propidium iodide, 200 µg/ml RNAse A and Triton X-100 in PBS) for 30 min at 37 °C. The DNA contents of more than 10000 cells were subjected to fluorescence-activated cell sorting (FACS) analysis (Coulter® Epics® XL™, Beckman) and the percentage of cells belonging to the different compartments of the cell cycle was determined. All experiments were performed in duplicate and reproduced at least two times.
Statistical analysis. Statistical analyses were performed using the Student's t-test to determine the differences between the datasets. Values of p lower than 0.05 were considered significant.

4.6. PCR Stop Assay

The stabilization of G4 structures by Salnaph complexes was investigated by PCR Stop Assay. The last G repeat of a test oligonucleotide (Pu22myc, GAGGGTGGGGAGGGTGGGGAAG) hybridizes with a partially complementary oligonucleotide (RevPu22, ATCGCTTCTCGTCTTCCCCA).
Assay reactions were performed in a final volume of 25 µl, 1X PCR buffer (Thermoscientific, 75 mM Tris-HCl, 20 mM $(NH_4)_2SO_4$, 0.1% (v/v) Tween 20), 1.5 mM $MgCl_2$, dNTPs 0.5 mM (each) 7.5 pmol of each oligonucleotide, 1.5 U of Taq DNA polymerase (recombinant) (Thermoscientific) and increasing concentrations of the tested ligand. Reaction mixtures were incubated in a thermocycler (MJ Research PTC-225-Tetrad PCR System) with the following cycle conditions: 94 °C for 5 minutes, followed by 35 cycles of 94 °C for 30 s, 58 °C for 30 s and 72 °C for 1 min, then a final step 72 °C for 10 minutes was run. The same reactions were performed by replacing the test oligonucleotide Pu22myc with a modified test oligonucleotide (Pu22mu, GAGGGTGGAAAGGGTGGGGAAG). Amplified products were loaded on 15% native polyacrylamide gels in 1X TBE buffer and run for 45 min at 180V. After staining for 10 min the gels in SYBR gold (Invitrogen), images were acquired by UV trans-illumination (UVITEC) and analyzed by the software Image J.

4.7. Computational details

Molecular Dynamics simulations. The interaction of the zinc(II) complex **3** with two different G4-DNA models, i.e. the *h-Telo* DNA (PDB ID 1KF1)[59] and the human *c-myc* promoter (PDB ID 1XAV),[60] was investigated by molecular dynamics (MD) simulations, by following a recently reported procedure.[35] In detail, four MD simulations were carried out, two for the two G4 models and two for the **3**/G4 complexes, through the GROMACS 4.5.3 software package,[61,62] of 50 ns and 150 ns in the case of **3**/*c-myc* complex, using the Amber99 force field[63] with Parmbsc0 nucleic acid torsions.[64,65] The zinc(II) complex **3** was positioned about 7 Å far over the 3' G-quartet in order to simulate the recognition process. The starting geometry and the partial atomic charges of the metal complex were obtained by DFT calculations (see below), while other intramolecular force-field parameters were generated with the ACPYPE software.[66–68] Triclinic box of TIP3P water molecules was added around the quadruplex to a depth of 1.5 nm on each side of the solutes to obtain a solution density of about 1.02 g/ml. 21 K^+ counterions (19 in the presence of the metal complex) were added to neutralize the negative charges of the phosphate groups, while other 17 K^+ and Cl^- ions were added to set the solution ionic strength to about 0.15 M (see Supporting Information, Fig. S2). Van der Waals parameters for zinc (=0.195998 nm =0.05230 kJ/mol) and chlorine (=0.440104 nm, =0.418400 kJ/mol) ions were taken from the Amber99 force field implemented in GROMACS, while those for potassium cation (=0.3410 nm, = 0.81091 kJ/mol) were taken from the literature.[69] Explicit solvent simulations were performed in the isothermal-isobaric NPT ensemble, at a temperature of 300 K, under control of a velocity rescaling thermostat.[70,71] The particle mesh Ewald method was used to describe long-range electrostatic interactions.[72] The timestep for integration was 2 fs and all covalent bonds, including the four bonds between the metal ion and the tetracoordinate Schiff-base ligand, constrained with the LINCS algorithm. There were two temperature coupling groups in these simulations, the first for the quadruplex and, if present, for the metal complex, the second for water and ions. Preliminary MD simulations showed that the structure of the isolated metal complex is maintained in solution. Preliminary energy minimizations were run for 5000 steps with the steepest descend algorithm. During the equilibration, the quadruplex and the metal complex/quadruplex system were harmonically restrained with a force constant of 1000 kJ mol^{-1} nm^{-2}, gradually relaxed

into five consecutive steps of 100 ps each, to 500, 200, 100 and 50 kJ mol^{-1} nm^{-2}.

DFT/MM calculations. The relaxed geometries of the *h-Telo* G4 model and its complex with **3** were used as starting structures to investigate the interaction of G4 with **1**, **2** and **3**, by two-layer quantum mechanics/molecular mechanics (QM/MM) hybrid calculations, as implemented in the ONIOM method,[73,74] with the aim to perform a high-level calculation on the complex stacked on the 3' G-quartet and to take account of the constraining effects of the quadruplex structure at a lower level of theory. Full geometry optimizations were performed, by using the M06-2X DFT functional[75] and the dzvp basis set,[76] in the higher QM layer[77] and the Amber99 force field in the lower MM layer of the DFT/MM calculations. The highest layer of the model includes the four guanine bases of the 3' G-quartet and the cationic complex, with charge set to +2 and spin multiplicity 1. Default atomic partial charges were used for the quadruplex atoms, implicitly included in the force field parameters.

Vibration frequency calculations, within the harmonic approximation, were performed on the optimized geometries by using the same DFT/MM method. Solvent effects were evaluated by performing M06-2X/dzvp single point calculations on the high layer model extracted by the DFT/MM optimized geometry, with the implicit water solvent reproduced by the polarizable continuum model (PCM),[78,79] using default settings for PCM cavities and an ultrafine integration grid. Standard enthalpy and Gibbs free energy values, at 298.15 K, of each energy minimum structure, both *in vacuo* and in solution, were calculated by adding the thermal correction obtained by vibration frequency analysis of the DFT/MM systems to the DFT energy calculated for the high layers (see Supporting Information, Table S1). The PCM energy data contain also non-electrostatic effects. Cartesian coordinates of the optimized structures are reported in the Supporting Information (Table S2). All calculations were performed by the Gaussian 09 program package.[80]

Conclusions

Detailed information on the binding of three square planar nickel(II) (**1**), copper(II) (**2**) and zinc(II) (**3**) Schiff-base complexes with G4-DNA was obtained through the complementary application of absorption, circular dichroism and gel electrophoresis investigations in water solution and computational studies, consisting of molecular dynamics simulations (MD) and quantum mechanics/molecular mechanics (DFT/MM) calculations.

The results obtained confirmed that **1**, **2** and **3** are strong G4-binders, with affinity decreasing in the order Ni > Cu ≈ Zn and with selective affinity of the three metal complexes toward G4-DNA compared to B-DNA. In particular, the nickel compound **1** binds G4-DNA 100 times stronger that B-DNA and that this value is among the highest reported in the literature.

MD simulations provided a possible interaction mechanism between the zinc complex **3** with both *c-myc* and *h-Telo* G4-DNA, while DFT/MM calculations provided detailed local information on the DNA-binding site and an explanation of the solvent and thermodynamics contributions in the binding with the biomolecules. In particular, the higher entropic destabilization following the formation of both **2**/*h-Telo* and **3**/*h-Telo*, compared to the **1**/*h-Telo* complex, follows the coordination of the apical empty site of the copper and zinc ions by the exocyclic keto-oxygen of a guanine base in the terminal G-tetrad, while the nickel ion maintains its square planar coordination geometry of the isolated Schiff-base complex. The values of the DNA-binding constants and their decreasing trend in the order **1** > **2** ≈ **3**, are correctly reproduced by the calculated formation Gibbs free energy values of the supramolecular complexes of **1**, **2** and **3** with *h-Telo* G4-DNA in solution.

CD and PCR experiments strongly suggest that complex **1** is able to induce the formation of G4-DNA at low concentration even in the absence of K^+ cations, confirming the possible different behavior of this compound as indicated by both spectroscopic and computational studies. Finally, the DNA binding results of the tested complexes nicely agree with their biological activity against HeLa and MCF-7 cancer cell lines. In details, the nickel complex **1** showed effective antiproliferative properties that decreases by following the same trend found in the G4-DNA binding studies.

Acknowledgements

We gratefully acknowledge University of Palermo for financial support, through the FFR 2012/2013 grant, and the CINECA award N. IsB07, year 2013, under the ISCRA initiative, for the availability of high performance computing resources and support. We thank members of the European COST Action CM1105 for stimulating discussions.

Abbreviations

CD: circular dichroism
c-myc: Avian myelocytomatosis virus oncogene cellular homolog
ct-DNA: calf thymus DNA
DFT/MM: density functional theory/molecular mechanics
DMEM: Dulbecco's Modified Eagle Medium
G4: G-quadruplex
Hela: human epithelial cervical cancer
h-Telo: Human Telomeric
MCF-7: human epithelial breast cancer
MD: molecular dynamics
PCR: polymerase chain reaction
RPMI: Roswell Park Memorial Institute medium
Tris-Hcl: tris-hydroxymethyl-aminomethane

Notes and references

[a] *Dipartimento di Scienze e Tecnologie Biologiche, Chimiche e Farmaceutiche, Viale delle Scienze, Edificio 17, 90128 Palermo, Italy. Fax: +39 091 596825; E-mail: giampaolo.barone@unipa.it*
[b] *Swedish Medical Nanoscience Center, Department of Neuroscience, Karolinska Institutet, Stockholm, Sweden;*
[c] *Istituto EuroMediterraneo di Scienza e Tecnologia, Via Emerico Amari 123, 90139 Palermo, Italy.*

† Electronic Supplementary Information (ESI) available: [Additional

figures (Figures S1-S3) and tables (Tables S1-S2), reporting PCR inhibition assays, DFT energies, *in vacuo* and in solution, thermal corrections, Cartesian coordinates. Video file showing the molecular dynamics of the binding between compound **3** and *c-myc* G4-DNA]. See DOI: 10.1039/b000000x/

1 B. Rosenberg, L. Van Camp, E.B. Grimley and A.J. Thomson, *J. Biol. Chem.* 1967, **242**, 1347–1350.
2 V. Brabec and J. Kasparkova, *Drug Resist. Updates* 2005, **8**, 131–146.
3 M.J. Hannon, *Chem. Soc. Rev.* 2007, **36**, 280–295.
4 B.M. Zeglis, V.C. Pierre and J.K. Barton, *Chem. Commun.* 2007, 4565–4579.
5 C. Ducani, A. Leczkowska, N.J. Hodges and M.J. Hannon, *Angew. Chem., Int. Ed.* 2010, **49**, 8942–8945.
6 A. Lauria, A. Terenzi, C. Gentile, A. Martorana, G. Gennaro, G. Barone and A. Almerico, *Lett. Drug Des. Discovery*. 2013, **11**, 15–26.
7 S. Neidle, *Nat. Prod. Rep.* 2001, **18**, 291–309.
8 S. Balasubramanian, L.H. Hurley and S. Neidle, *Nat. Rev. Drug Discov.* 2011, **10**, 261–275.
9 P. Cohen, *Nat. Rev. Drug Discov.* 2002, **1**, 309–315.
10 A. Pace, G. Barone, A. Lauria, A. Martorana, A.P. Piccionello, P. Pierro, A. Terenzi, A.M. Almerico, S. Buscemi, C. Campanella, F. Angileri, F. Carini, G. Zummo, E.C. de Macario, F. Cappello and A.J.L. Macario, *Curr. Pharm. Des.* 2013, **19**, 2757–2764.
11 A. Lauria, I. Abbate, C. Gentile, F. Angileri, A. Martorana and A.M. Almerico, *J. Med. Chem.* 2013, **56**, 3424–3428.
12 A. Lauria, M. Ippolito and A.M. Almerico, *Comput. Biol. Chem.* 2009, **33**, 386–390.
13 D. Sen and W. Gilbert, *Nature* 1988, **334**, 364–366.
14 W.I. Sundquist and A. Klug, *Nature* 1989, **342**, 825–829.
15 A.M. Zahler, J.R. Williamson, T.R. Cech and D.M. Prescott, *Nature* 1991, **350**, 718–720.
16 D. Yang and K. Okamoto, *Future Med. Chem.* 2010, **2**, 619–646.
17 G.W. Collie and G.N. Parkinson, *Chem. Soc. Rev.* 2011, **40**, 5867–5892.
18 T.M. Bryan and P. Baumann, *Mol. Biotechnol.* 2011, **49**, 198–208.
19 A.G. Bodnar, Science. 1998, **279**, 349–352.
20 N.H. Campbell, N.H.A. Karim, G.N. Parkinson, M. Gunaratnam, V. Petrucci, A.K. Todd, R. Vilar and S. Neidle, *J. Med. Chem.* 2012, **55**, 209–222.
21 J.L. Huppert and S. Balasubramanian, *Nucl. Acids Res.* 2005, **33**, 2908–2916.
22 C.V. Dang, L.M.S. Resar, E. Emison, S. Kim, Q. Li, J.E. Prescott, D. Wonsey and K. Zeller, *Exp. Cell Res.* 1999, **253**, 63–77.
23 T.-M. Ou, Y.-J. Lu, C. Zhang, Z.-S. Huang, X.-D. Wang, J.-H. Tan, Y. Chen, D.-L. Ma, K.-Y. Wong, J.C.-O. Tang, A.S.-C. Chan and L.-Q. Gu, *J. Med. Chem.* 2007, **50**, 1465–1474.
24 T.A. Brooks, S. Kendrick and L. Hurley, *FEBS J.* 2010, **277**, 3459–3469.
25 S. Millevoi, H. Moine and S. Vagner, *Wiley Interdiscip. Rev.: RNA* 2012, **3**, 495–507.
26 H. Han and L.H. Hurley, *Trends Pharmacol. Sci.* 2000, **21**, 136–142.
27 S.N. Georgiades, N.H. Abd Karim, K. Suntharalingam and R. Vilar, *Angew. Chem., Int. Ed.* 2010, **49**, 4020–4034.
28 A. Arola-Arnal, J. Benet-Buchholz, S. Neidle and R. Vilar, *Inorg. Chem.* 2008, **47**, 11910–11919.
29 S.M. Haider, G.N. Parkinson and S. Neidle, *J. Mol. Biol.* 2003, **326**, 117–125.
30 G. Barone, N. Gambino, A. Ruggirello, A. Silvestri, A. Terenzi and V.T. Liveri, *J. Inorg. Biochem.* 2009, **103**, 731–737.
31 A. Terenzi, C. Ducani, L. Male, G. Barone and M.J. Hannon, *Dalton Trans.* 2013, **42**, 11220.
32 A. Silvestri, G. Barone, G. Ruisi, D. Anselmo, S. Riela and V.T. Liveri, *J. Inorg. Biochem.* 2007, **101**, 841–848.
33 J.E. Reed, A. Arola-Arnal, S. Neidle and R. Vilar, *J. Am. Chem. Soc.* 2006, **128**, 5992–5993.
34 N.H. Abd Karim, O. Mendoza, A. Shivalingam, A.J. Thompson, S. Ghosh, M.K. Kuimova and R. Vilar, *RSC Adv.* 2014, **4**, 3355–3363.
35 A. Lauria, R. Bonsignore, A. Terenzi, A. Spinello, F. Giannici, A. Longo, A.M. Almerico and G. Barone, *Dalton Trans.* 2014, **43**, 6108-6119
36 R. Kieltyka, J. Fakhoury, N. Moitessier and H.F. Sleiman, *Chem.-Eur. J.* 2008, **14**, 1145–1154.
37 G. Barone, A. Terenzi, A. Lauria, A.M. Almerico, J.M. Leal, N. Busto and B. García, *Coord. Chem. Rev.* 2013, **257**, 2848–2862.
38 M.T. Record, C.F. Anderson and T.M. Lohman, *Q. Rev. Biophys.* 1978, **11**, 103–178.
39 T. Uno, K. Hamasaki, M. Tanigawa and S. Shimabayashi, *Inorg. Chem.* 1997, **36**, 1676–1683.
40 A. Terenzi, L. Tomasello, A. Spinello, G. Bruno, C. Giordano and G. Barone, *J. Inorg. Biochem.* 2012, **117**, 103–110.
41 B.R. Vummidi, J. Alzeer and N.W. Luedtke, *ChemBioChem* 2013, **14**, 540–558.
42 M. Read, R.J. Harrison, B. Romagnoli, F.A. Tanious, S.H. Gowan, A.P. Reszka, W.D. Wilson, L.R. Kelland and S. Neidle, *Proc. Natl. Acad. Sci. U. S. A.* 2001, **98**, 4844–4849.
43 M.J. Waring, *J. Mol. Biol.* 1965, **13**, 269–274.
44 A.I. Karsisiotis, N.M. Hessari, E. Novellino, G.P. Spada, A. Randazzo and M. Webba da Silva, *Angew. Chem., Int. Ed.* 2011, **50**, 10645–10648.
45 S. Paramasivan, I. Rujan and P.H. Bolton, *Methods.* 2007, **43**, 324–331.
46 S. Masiero, R. Trotta, S. Pieraccini, S. De Tito, R. Perone, A. Randazzo and G.P. Spada, *Org. Biomol. Chem.* 2010, **8**, 2683–2692.
47 K. Suntharalingam, A.J.P. White and R. Vilar, *Inorg. Chem.* 2009, **48**, 9427–9435.
48 J. Zhou and G. Yuan, *Chem.-Eur. J.* 2007, **13**, 5018–5023.
49 D.P.N. Gonçalves, S. Ladame, S. Balasubramanian and J.K.M. Sanders, *Org. Biomol. Chem.* 2006, **4**, 3337–3342.
50 E.M. Rezler, J. Seenisamy, S. Bashyam, M.-Y. Kim, E. White, W.D. Wilson and L.H. Hurley, *J. Am. Chem. Soc.* 2005, **127**, 9439–9447.
51 P. Wu, D.-L. Ma, C.-H. Leung, S.-C. Yan, N. Zhu, R. Abagyan and C.-M. Che, *Chem.-Eur. J.* 2009, **15**, 13008–13021.
52 A. Spinello, A. Terenzi and G. Barone, *J. Inorg. Biochem.* 2013, **124**, 63–69.
53 M. Aleksić, B. Bertoša, R. Nhili, L. Uzelac, I. Jarak, S. Depauw, M.-H. David-Cordonnier, M. Kralj, S. Tomić and G. Karminski-Zamola, *J. Med. Chem.* 2012, **55**, 5044–5060.
54 T. Mosmann, *J. Immunol. Methods* 1983, **65**, 55–63.
55 A. Siddiqui-Jain, C.L. Grand, D.J. Bearss and L.H. Hurley, *Proc. Natl. Acad. Sci. U. S. A.* 2002, **99**, 11593–11598.
56 T. Lemarteleur, D. Gomez, R. Paterski, E. Mandine, P. Mailliet and J.-F. Riou, *Biochem. Biophys. Res. Commun.* 2004, **323**, 802–808.
57 P. McPhie, *Methods Enzymol.* 1971, **22**, 23–32.
58 S.D. Kennedy and R.G. Bryant, *Biophys. J.* 1986, **50**, 669–676.
59 G.N. Parkinson, M.P.H. Lee and S. Neidle, *Nature* 2002, **417**, 876–880.
60 A. Ambrus, D. Chen, J. Dai, R.A. Jones and D. Yang, *Biochemistry* 2005, **44**, 2048–2058.
61 D. Van Der Spoel, E. Lindahl, B. Hess, G. Groenhof, A.E. Mark and H.J.C. Berendsen, *J. Comput. Chem.* 2005, **26**, 1701–1718.
62 B. Hess, C. Kutzner, D. van der Spoel and E. Lindahl, *J. Chem. Theory Comput.* 2008, **4**, 435–447.
63 J. Wang, P. Cieplak and P.A. Kollman, *J. Comput. Chem.* 2000, **21**, 1049–1074.
64 A. Pérez, I. Marchán, D. Svozil, J. Sponer, T.E. Cheatham III, C.A. Laughton and M. Orozco, *Biophys. J.* 2007, **92**, 3817–3829.
65 A.T. Guy, T.J. Piggot and S. Khalid, *Biophys. J.* 2012, **103**, 1028–1036.
66 A.W. Sousa Da Silva, W.F. Vranken and E.D. Laue, ACPYPE - Antechamber Python Parser Interface, http://code.google.com/p/acpype.
67 J. Wang, R.M. Wolf, J.W. Caldwell, P.A. Kollman and D.A. Case, *J. Comput. Chem.* 2004, **25**, 1157–1174.
68 J. Wang, W. Wang, P.A. Kollman and D.A. Case, *J. Mol. Graphics Model.* 2006, **25**, 247–260.
69 I.S. Joung and T.E. Cheatham, *J. Phys. Chem. B* 2008, **112**, 9020–9041.
70 G. Bussi, D. Donadio and M. Parrinello, *J. Chem. Phys.* 2007, **126**, 014101–014101–7.
71 M. Parrinello and A. Rahman, *J. Appl. Phys.* 1981, **52**, 7182–7190.
72 T. Darden, D. York and L. Pedersen, *J. Chem. Phys.* 1993, **98**, 10089–10092.
73 M. Svensson, S. Humbel, R.D.J. Froese, T. Matsubara, S. Sieber and K. Morokuma, *J. Phys. Chem.* 1996, **100**, 19357–19363.

74 T. Vreven and K. Morokuma, *J. Comput. Chem.* 2000, **21**, 1419–1432.
75 Y. Zhao and D.G. Truhlar, *Theor. Chem. Acc.* 2008, **120**, 215–241.
76 N. Godbout, D.R. Salahub, J. Andzelm and E. Wimmer, *Can. J. Chem.* 1992, **70**, 560–571.
77 A. Spinello, A. Terenzi and G. Barone, *J. Inorg. Biochem.* 2013, **124**, 63–69.
78 J. Tomasi, B. Mennucci and R. Cammi, *Chem. Rev.* 2005, **105**, 2999–3093.
79 G. Scalmani and M.J. Frisch, J. Chem. Phys. 2010, **132**, 114110.
80 M. Frisch, G. Trucks, H. Schlegel, G. Scuseria, M. Robb, J. Cheeseman, G. Scalmani, V. Barone, B. Mennucci, G. Petersson, H. Nakatsuji, M. Caricato, X. Li, H. Hratchian, A. Izmaylov, J. Bloino, G. Zheng, J. Sonnenberg, M. Hada, M. Ehara, K. Toyota, R. Fukuda, J. Hasegawa, M. Ishida, T. Nakajima, Y. Honda, O. Kitao, H. Nakai, T. Vreven, J. Montgomery, J. Peralta, F. Ogliaro, M. Bearpark, J. Heyd, E. Brothers, K. Kudin, V. Staroverov, R. Kobayashi, J. Normand, K. Raghavachari, A. Rendell, J. Burant, S. Iyengar, J. Tomasi, M. Cossi, N. Rega, J. Millam, M. Klene, J. Knox, J. Cross, V. Bakken, C. Adamo, J. Jaramillo, R. Gomperts, R. Stratmann, O. Yazyev, A. Austin, R. Cammi, C. Pomelli, J. Ochterski, R. Martin, K. Morokuma, V. Zakrzewski, G. Voth, P. Salvador, J. Dannenberg, S. Dapprich, A. Daniels, Farkas, J. Foresman, J. Ortiz, J. Cioslowski, and D. Fox, *Gaussian 09 Revis. A1 Gaussian Inc Wallingford CT*, 2009.